This is a repository copy of *Longitudinal dispersion in unsteady pipe flows*.

White Rose Research Online URL for this paper:
https://eprints.whiterose.ac.uk/175105/

Version: Accepted Version

Article:

1   # Longitudinal Dispersion in Unsteady Pipe Flows

2   James Hart, Fred Sonnenwald, Virginia Stovin and Ian Guymer

3   ## Abstract

4   Temporal concentration profiles resulting from an injected pulse of fluorescent tracer were recorded
5   at multiple locations along a pipe during controlled unsteady flow conditions. A linear temporal
6   change in discharge over durations of 5, 10, or 60 s for both accelerating and decelerating flow
7   conditions was studied. Tests were performed for flows that changed within the turbulent range,
8   between Reynolds numbers of 6,500 and 47,000, and for laminar to turbulent flows, between
9   Reynolds numbers of 2,700 and 47,000. Analysis of the data shows the limitations of employing
10   steady-state routing of temporal concentration profiles in unsteady flows. Employing a 'flow
11   weighted time' routing approach, using tracer mean velocity and dispersion coefficients, provides
12   accurate predictions of mixing in unsteady flow. For decelerating flows, longitudinal dispersion
13   coefficients were lower than for the equivalent mean steady discharge. Previously unreported
14   disaggregation of the tracer cloud was observed during all experiments accelerating from laminar to
15   turbulent conditions.

16   ## Introduction

17   It is important to understand the fate of solutes in drinking water supply networks. Examples include
18   disinfectants introduced into the network by the operator, or contaminants that unintentionally find
19   their way into the network. Basha and Malaeb (2007) highlight the importance of including dispersion
20   effects, especially in low velocity pipes. The ability to model the mixing of these solutes, and
21   therefore predict the peak concentration and longitudinal spread at downstream locations, is
22   required to ensure water quality throughout the network.

23   Water mains and central regions of water supply networks operate under conditions of steady,
24   turbulent flow, where theory derived from Taylor's original analysis (Taylor, 1954) is sufficient to
25   estimate dispersion. However, local regions of the distribution network, where water leaves the main
26   network, often experience much lower discharges, and conditions in these regions have been shown
27   to be turbulent, transitional or even laminar (Buchberger et al., 2003). Furthermore, as discharge is a
28   function of local, intermittent demand, flows can also be highly time varied and do not necessarily
29   hold to the steady flow assumption (Buchberger et al., 2003). The aim of this paper is to
30   experimentally investigate longitudinal dispersion in unsteady flow and to assess the degree to which
31   solute transport routing can be applied and extended to unsteady flows of different acceleration
32   durations.

33   The fundamental fluid dynamics for unsteady pipe flows have been studied in the laboratory by
34   several authors. Kurokawa and Morikawa (1986) investigated the effect of acceleration and
35   deceleration on pipe flow by measuring temporal velocity profiles at different radial locations using
36   hot wire anemometer. The flow was either accelerated or decelerated between stationary
37   conditions (i.e. Re = 0) and a discharge corresponding to Re = 73,000. A range of acceleration and
38   deceleration durations was investigated. Figure 1, reproduced from Kurokawa and Morikawa (1986)
39   in simplified form, shows the temporal variation in velocity at four radial positions (y/r), where y is
40   the distance from the pipe wall and r is the pipe radius. The results from the maximum and
41   minimum acceleration durations studied, 2.5 s and 25 s, are shown in Figure 1a and 1b respectively.
42   As the flow accelerates from stationary conditions, a point of transition can be seen in both time
43   series between the centreline and pipe boundary regions. Around this transition, the central core of
44   the flow ($y/r \geq 0.50$) exhibits a smoother acceleration compared to the flow closer to the pipe

45   boundary (y/r < 0.50). These transitions occur at different times and Reynolds numbers, depending
46   on the acceleration duration, and in both cases the transition velocity is higher than it would be for
47   the transition from laminar to turbulent flow to occur under steady flow conditions. Around the
48   transition there is a rapid temporal change, and spatial differences in velocity of up to 100% were
49   recorded. This period of non-equilibrium will impact on the longitudinal mixing of solutes within the
50   flow.

51   He and Jackson (2000) measured velocity profiles in turbulent, unsteady pipe flow using a two-
52   component LDA system. For the main test series, they considered fully turbulent flows which were
53   accelerated or decelerated between Reynolds Numbers of 7,000 and 45,200 and considered the
54   effects of acceleration duration on the velocity profile in terms of a dimensionless ramp rate
55   parameter. This parameter allowed the authors to quantify whether the flow was equivalent to fully
56   developed steady flow at each discrete cross-sectional velocity, a case deemed 'pseudo-steady flow'.
57   In the slowest acceleration, with an acceleration duration of 45 s, the velocity profiles showed no
58   difference between measured and predicted steady flow profiles. In contrast, during the early stages
59   of the fastest acceleration, over 5 s, the velocity was measured to be slightly lower than the 'pseudo-
60   steady velocity' values near the pipe centre and slightly higher close to the pipe boundary. The
61   magnitude of these differences was < 10%, much less than differences recorded by Kurokawa and
62   Morikawa (1986).

63   Greenblatt and Moss (2004) measured velocity profiles, using 1D LDA in transient water pipe flow
64   and considered three acceleration durations, all shorter than the previous studies of Kurokawa and
65   Morikawa (1986) and He and Jackson (2000). The acceleration durations were around 0.5, 1.25 and
66   2.5 s and for all cases considered, the flow was always turbulent with an initial Reynolds number of
67   31,000 and a final value of 82,000. Profile parameters exhibited similar qualitative trends to one
68   another when time was scaled with the acceleration duration and this differed from corresponding
69   spatial development of flows subjected to steady streamwise pressure gradients.

70   In summary, previous studies highlight that, for long acceleration durations, unsteady pipe flow can
71   be approximated by a steady flow model. In contrast, for short acceleration durations, the
72   approximation becomes less accurate. This is most clearly illustrated as the flow accelerates from
73   laminar to fully turbulent in the results from Kurokawa and Morikawa (1986), Figure 1, which show
74   significant discontinuities occurring in the radial velocity profile for a rapid acceleration. Given the
75   effects of flow acceleration on the hydrodynamics, this paper investigates how these impact on
76   solute mixing.

77   Longitudinal dispersion for steady pipe flow was initially investigated by Taylor (1953, 1954), who
78   showed that after an initial period required for the solute to become cross-sectionally well mixed,
79   the longitudinal distribution of the solute's cross-sectional mean concentration will be Gaussian.
80   Shear dispersion is the result of radial variations of the velocity profile. Initially after injection, shear
81   effects are out of balance with pure advection, which impart considerable skewness to the
82   concentration profile. After an initial period, long enough for the contaminant to experience the
83   complete flow field, a balance is established between the processes of shear dispersion and
84   molecular or turbulent diffusion. Analysis by Chatwin (1970) has shown that the time scale to
85   become cross-sectionally well-mixed is ≈ $0.2r^2/D_m$ where D_m is the molecular diffusion coefficient.
86   This is an order of magnitude greater than that estimated by Taylor (1954). Following the initial
87   period, the variance of the concentration profiles increases linearly with time and the skewness
88   decreases. Through Taylor's analysis, the effects of dispersion in a pipe can be modelled by a
89   gradient diffusion term. The area averaged one-dimensional form of the advection dispersion
90   equation (ADE) used for longitudinal mixing is:

$$\frac{\partial c}{\partial t} + u\frac{\partial c}{\partial x} = D\frac{\partial^2 c}{\partial x^2} \qquad (1)$$

91

92   where c is concentration, t is time, x is longitudinal distance, u is velocity and D is the longitudinal
93   dispersion coefficient accounting for the mixing processes: molecular and turbulent diffusion and
94   shear dispersion. Assuming an instantaneous injection, Equation 1 can be solved to give the
95   concentration profile downstream in a pipe after a given period of time as:

$$c(x,t) = \frac{M}{A\sqrt{4\pi Dt}}exp\left(-\frac{(x-ut)^2}{4Dt}\right) \qquad (2)$$

96

97   where A is cross-sectional area and M is mass of injected contaminant (Fischer et al., 1979). This
98   solution provides concentration distributions as a function of longitudinal distance at discrete times,
99   i.e. a snapshot in time, showing the spatial distribution of the contaminant.

100   Many practical modelling situations require the prediction of a downstream temporal concentration
101   profile, $c(x_2,t)$ from a known upstream profile, $c(x_1,t)$, where x_1 and x_2 are upstream and
102   downstream measurement locations respectively. In such situations, it is possible to use a routing
103   procedure solution to the ADE (Equation 5.20, Fischer et al., 1979). After applying the 'frozen cloud'
104   approximation by substituting $x = ut$, replacing M with the upstream concentration profile and
105   convolving Equation 2 with respect to time, the routing solution to the ADE is:

$$c(x_2,t) = \int_{\gamma=-\infty}^{\infty} \frac{c(x_1,\gamma)u}{\sqrt{4\pi D\bar{t}}}\exp\left[-\frac{u^2(\bar{t}-t+\gamma)^2}{4D\bar{t}}\right]d\gamma \qquad (3)$$

106

107   where $\bar{t}$ is travel time, the difference in time between the centroids of the upstream and
108   downstream concentration profiles and γ is an integration variable representing time. Equation 3
109   assumes steady-state conditions and predicts a downstream temporal concentration profile based
110   on a known upstream profile.

111   Taylor proposed two expressions for the longitudinal dispersion coefficient, one for laminar and
112   another for turbulent pipe flow. Taylor's expression for the dispersion coefficient within laminar flow
113   was derived assuming a parabolic velocity profile, whereas for turbulent flow he assumed a
114   logarithmic velocity profile, typical of highly turbulent flow. Following Taylor's work, as shown in
115   Hart et al. (2016), several other authors recorded data that demonstrated deviation between
116   experimentally obtained dispersion coefficients and Taylor's expression for Reynolds numbers (*Re*)
117   below 20,000. This deviation is due to the increasing significance of the boundary layer for *Re* <
118   20,000, causing increased longitudinal differential advection that is not accounted for by Taylor's
119   assumption of a logarithmic velocity profile with no boundary layer (Hart et al., 2013).

120   Whilst Taylor's expression, which assumes the solute to be well mixed and in equilibrium, is valid for
121   laminar flow, Hart et al. (2016) showed that it is not applicable in practice. In laminar flow, where
122   the only radial exchange is that of molecular diffusion, well-mixed conditions can take the order of
123   days or even weeks to develop in standard water distribution-sized pipes. Hart et al. (2016)
124   suggested an alternative approach based on the Residence Time Distribution (RTD) (Danckwerts,
125   1953). This approach was shown to vastly improve the prediction of the downstream temporal
126   concentration profile for Re < 3,000 at short times from injection.

127   Romero-Gomez and Choi (2011) provide additional evidence that the standard approach of Taylor
128   can be improved upon in laminar flow systems. For water supply systems, they developed and
129   experimentally verified a direction-dependent approach, giving forwards and backwards dispersion
130   rates. The approach demonstrated an improvement over the conventional formula using various
131   combinations of pipe lengths, tracer injections, mean flow velocities, and solute properties. Piazza et

132   al. (2020) employed the approach of Romero-Gomez and Choi (2011) within an EPANET water
133   distribution network model to show the importance of diffusive processes when the velocity is low.

134   Hart et al. (2016) showed that, although Taylor's expression for longitudinal dispersion coefficient for
135   turbulent flow with Re < 20,000 was unsuitable, the magnitude of the dispersion coefficient could be
136   corrected to account for the lower Reynolds Number effects. This enabled acceptable predictions of
137   concentration profiles for both transitional and turbulent flow. In the range 3,000 < Re < 50,000,
138   Hart et al. (2016) confirmed that D/ud was a function of Reynolds number, and proposed that for
139   their pipe system the longitudinal dispersion coefficient could be estimated from

140
$$\frac{D}{ud} = 1.17 \text{x} 10^9 Re^{-2.5} + 0.41 \tag{4}$$

141   where d is the pipe diameter.

142   Residence Time Distribution (RTD) theory (Levenspiel, 1972) introduced the concept of
143   dimensionless time, which is used to remove the effects of flow rate and volume when comparing
144   the mixing responses of different systems under different conditions. Nauman (1969) investigated
145   unsteady mixing processes in stirred tank reactors using RTDs and showed that RTD principles apply
146   to unsteady flow systems, including dimensionless time. Whilst Nauman (1969) used mean flow rate
147   when calculating dimensionless time, Fernandez-Sempere et al. (1995) examined RTDs from an
148   unsteady sewerage system using a dimensionless time parameter, ϕ. This is based on cumulative
149   volume over a constant system volume, where

150
$$\phi(t) = V^{-1} \int_0^t Q(\gamma) \mathrm{d}\gamma \tag{5}$$

151   where V is system volume (the volume of water between measurement locations) and Q the flow
152   rate.

153   For stormwater treatment systems, Werner & Kadlec (1996) investigated the concept of a
154   dimensionless time based on volume in more detail, naming ϕ 'flow weighted time'. They illustrated
155   the differences between RTDs obtained for the same system, depending on injection time in
156   unsteady flow, and showed that these differences were significantly minimised in flow weighted
157   time. Werner & Kadlec (1996) analysed the RTD in flow weighted time concept and showed the RTD
158   to have 0th and 1st moments of 1.0. This is desirable as it shows that the unsteady, or flow weighted
159   time RTD has many of the same statistical properties as the conventional steady RTD confirming the
160   results of Nauman (1969). The flow weighted time concept has since been used to analyse
161   concentrations across a range of unsteady flow problems (Leclerc et al., 2000, Wahl et al., 2012, and
162   Holland et al., 2004).

163   The aim of the present paper is to extend the application of flow weighted time-based analysis for
164   application to the prediction of longitudinal dispersion in unsteady pipe flows. The work is
165   underpinned by new laboratory data that quantifies longitudinal dispersion in a pipe subjected to
166   unsteady conditions. We propose a new form of the solute transport routing equation based on
167   flow weighted time, and test its application to the laboratory data through the estimation of
168   longitudinal dispersion coefficients from the laboratory data.

169   ## Methodology

170   *Experimental Methodology*

171   In water supply networks, a wide range of discharge patterns can be experienced. However, as one
172   of the first studies into the phenomena, this paper will only consider the case of flow accelerated or
173   decelerated at a constant gradient from an initial steady discharge to a final steady discharge.

174 The experimental results presented here were collected in the same laboratory rig used by Hart et
175 al. (2016). A simplified schematic of the set-up on the 24 mm diameter pipe is provided in Figure 2.
176 During some preliminary tracer tests, multiple concentration peaks were recorded at these
177 instrument locations. Hence, the previous experimental configuration was modified to confirm the
178 profile of the injected tracer cloud by locating an additional Turner Designs Series 10 fluorimeter
179 0.5 m downstream from the injection point. This is shown in Figure 2. Due to the close proximity of
180 this instrument to the injection location, the peak tracer concentration here was greater than the
181 maximum that could be recorded in some cases.

182 Unlike the steady flow study described by Hart et al. (2016), this series of experiments was
183 conducted with a linear temporal change in discharge over durations of 5, 10, or 60 s. A schematic of
184 the flow and test conditions is provided in Figure 3. The instantaneous discharge was measured
185 using an electromagnetic flow meter (Siemens Sitrans FM Mago MAG 5100W) and logged at 30 Hz.
186 For each run, an initial steady discharge was set to provide a predefined initial Reynolds number, Re_i
187 and injection (1) made, shown by the left-hand grey shaded area in Figure 3. The discharge was then
188 accelerated, or decelerated (negative acceleration), at a constant rate, to a final discharge and
189 Reynolds number, Re_f, with further tracer injections made during the unsteady discharge. A single
190 injection (Figure 3, injection 2) was made during each of the 5 and 10 s acceleration durations, with
191 two injections (2 & 3) possible during the longest, 60 s acceleration duration. A further injection (4),
192 was made into the final steady discharge. Discharge was controlled by the pump's digital controller
193 on the basis of a pre-set gradient. 1 s duration tracer injections were made using a peristaltic pump
194 at set times within the discharge acceleration.

195 Accelerating and decelerating flow conditions were investigated under turbulent flow conditions,
196 between Re_i & Re_f values of 6,500 & 47,000 (Tests 1 and 2), and between laminar and turbulent
197 conditions, between Re_i & Re_f values of 2,700 & 47,000 (in Tests 3 and 4). All traces were repeated
198 five times, resulting in 220 individual injections, each recorded by the 7 fluorimeters between 0.5
199 and 13.05 m downstream. Unfortunately, the fluorimeter positioned 10.98 m downstream of the
200 injection exhibited significant noise in the output and as a result, none of the data from this
201 fluorimeter has been included. In total, eighty individual traces were performed during transient
202 flow conditions from injections 2 and 3, and a summary of the test conditions is provided in Table 1.

203 ### *Extending the Routing Approach for Unsteady Flow*

204 The standard routing procedure solution to the ADE equation uses distance or time in steady flow
205 conditions, employing the frozen cloud approximation to convert between spatial and temporal
206 variations (Fischer et al., 1979). In unsteady flows, Eulerian measurements of concentration within a
207 system do not exhibit a linear increase in temporal variance with distance, which prevents the use of
208 the frozen cloud approximation for the determination of longitudinal dispersion coefficients. Here,
209 we propose to use flow weighted time (Werner & Kadlec, 1996) to extend the routing procedure
210 solution to the standard ADE and apply it to unsteady flow conditions.

211 The solute transport routing equation in dimensionless flow weighted time, ϕ, can be derived from
212 the standard solution Equation 2, again using an analogue of the frozen cloud approximation, letting
213 $\phi \simeq x$. By definition, both travel time and velocity (as units travelled per unit time) are 1 in flow
214 weighted time. Thus, as with the solution for Equation 3, after substitution for ϕ, $\bar{t}$, and u, Equation
215 2 is convolved with the upstream profile and the flow weighted time routing equation is therefore:

216
$$S(x_2, \phi) = \int_{\gamma - \infty}^{\infty} \frac{S(x_1, \gamma)}{\sqrt{4\pi J}} \exp\left[\frac{(1 + \gamma - \phi)^2}{4J}\right] d\gamma \qquad (6)$$

217 where $S(x_1, \gamma)$ and $S(x_2, \phi)$ are the upstream and downstream concentration profiles in flow
218 weighted time, J is the dimensionless flow weighted time dispersion coefficient, and γ is an
219 integration variable representing flow weighted time. Following dimensional analysis J is given as:

220
$$J = \frac{D}{us} \qquad (7)$$

221 where $s = x_2 - x_1$ is the distance between measurement points. Flow weighted time is an adjusted
222 time-axis where "time is stretched and compressed" (Werner & Kadlec, 1996), and since both u and
223 s affect the travel time, they are appropriate non-dimensionalisation parameters. Although Equation
224 6 is in dimensionless units of flow weighted time, it otherwise has the same interpretation of the
225 standard routing solution Equation 3. That is, each portion of the upstream profile is advected
226 downstream and spread out . The sum of these downstream components gives the final
227 downstream profile.

Analysis of the Experimental Data

229 Following calibration, the removal of background concentrations and the identification of the start
230 and end times of each trace, the temporal concentration profiles at each fluorimeter were analysed.
231 Results from injections in steady flow conditions (recorded before and after injections in unsteady
232 flow) were compared to the values obtained by Hart et al. (2016) and showed good agreement.

233 The new data analysis presented here focuses on the two injections (Injections 2 and 3) made during
234 the unsteady phase of each test. This paper presents the data recorded by all the fluorimeters to
235 illustrate the processes. However, for quantifying longitudinal dispersion coefficients, to ensure that
236 all the measurements analysed were obtained during the unsteady transient flow conditions, the
237 study reach used is restricted to the 4.4 m length of pipe between fluorimeters located at 2.68 m
238 and 7.08 m.

239 We first apply Equation 3, the traditional steady-state routing of temporal concentration profiles in
240 actual time, hereafter referred to as 'temporal routing', to the study reach data. We then similarly
241 apply Equation 6, solute routing in flow weighted time, hereafter referred to as 'flow weighted
242 routing'. In both cases we use the previously published (Hart et al., 2016) steady state dispersion
243 coefficient relationship, Equation 4, although for the latter converted using Equation 7. Finally, we
244 quantify the dimensionless longitudinal dispersion coefficient and mean travel time through least-
245 squares optimisation of Equation 6 to the measured data, producing 'optimised' values. Goodness-
246 of-fit has been quantified using the R_t^2 correlation coefficient (Young et al., 1980). Mean values
247 derived from five repeat tests were determined in each case, whilst the data presented in the figures
248 is from the first of the repeat injections.

Results

Recorded Trace Data

251 Figures 4a & 5a show the recorded temporal concentration profiles, for accelerating flow conditions,
252 from each of the six fully operational fluorimeters. Also plotted are the temporal variations of
253 Reynolds number and cumulative volume, both calculated from the instantaneous flow meter
254 output. Figure 4a shows results from Test 1 with a 5 s acceleration duration, where the flow is
255 always turbulent. Figure 5a shows results from the early injection (2) in Test 3, performed for a 60 s
256 acceleration, where the flow is accelerating from laminar to turbulent. Figures 4b & 5b show the
257 temporal concentration profiles with the peak concentration values centred on zero. Under these
258 accelerating flow conditions, the temporal concentration profiles do not show an increase in spread
259 with distance or travel time. On the contrary, a reduction in spread with distance is observed due to

260 the accelerating flow conditions. Considering the concentration profiles in flow weighted time,
261 Figures 4c & 5c, again centring the peaks at zero, show a clear, systematic increase in spread with
262 distance from injection, in agreement with standard dispersion theory. This confirms the
263 applicability of the flow weighted time approach.

264 Note that in Figures 4c and 5c, the flow weighted time was calculated using the cumulative volume
265 for the entire test, together with the system volume of the study reach. Normally each reach would
266 be examined with its own flow weighted time, leading to each trace being stretched/squeezed to fit
267 a flow weighted travel time of 1. However, such a manipulation would mask the increasing spread
268 with distance from injection.

269 Figure 5 shows multiple peaks in the temporal concentration profiles at all measurement locations
270 other than for the fluorimeter at x = 0.50 m. This 'disaggregation' of the upstream single peak to
271 multiple downstream peaks is evident in all injection 2 traces recorded in Test 3. This novel
272 observation will be fully addressed in the Discussion section.

273 The time of the centroid of each temporal concentration profile has been used to characterise the
274 flow conditions under which each of these traces was recorded. In Table 1, columns 1 & 2
275 summarise the test numbers and the acceleration durations, with injection number, 2 or 3, shown in
276 column 3. Columns 4 and 5 present the values of the instantaneous Reynolds numbers at the
277 centroid times for the upstream and downstream temporal concentration profiles at 2.68 m and
278 7.08 m respectively, with the temporal mean value given in column 6. Despite Test 3 commencing
279 during laminar flow conditions, all the traces analysed through the study reach were performed with
280 mean Reynolds numbers denoting turbulent flow. Average values for the accelerating flow tests, 1
281 and 3, were around 31,000, apart from injection 2 for the 60 s acceleration duration which had
282 values of approximately 12,500. Average Reynolds numbers for the decelerating flows tests, 2 and 4,
283 for injection 2 were around 44,750, with injection 3 having smaller values of around 25,000.
284 Comparing flow conditions across the five repeat injections in all traces, they showed little variation;
285 the standard deviation in Re was always $\leqslant$ 1,200, with an average standard deviation of 200.

286 *Temporal routing*

287 This section examines the ability of the standard steady-state temporal routing approach to predict
288 downstream concentrations in unsteady flow conditions in actual time (Equation 3). The travel time
289 (from tracer mean velocity) and dispersion coefficients (from Equation 4) were obtained from the
290 equivalent mean steady flow conditions. Sample results from the first of the repeat injections for all
291 the Tests for 5 s, 10 s and 60 s acceleration duration, with both early and late injection, are shown in
292 Figures 6 to 9 respectively. The predicted temporal concentration profiles for 5 s, 10 s and 60 s
293 acceleration durations are shown by the red chain dashed line for all the tests. The secondary x axis
294 shows 10% increments of flow weighted time, to illustrate how rapidly the flow changed. The results
295 show the measured downstream concentration profiles at 7.08 m (grey filled circles). The blue and
296 black dashed lines in Figures 6 to 9 will be discussed in the following sections. R_t^2 values (denoted *t*)
297 are given in the upper right corner. The mean quality of the fit of the temporal routing predictions
298 has an R_t^2 value of 0.785.

299 For the majority of conditions, the predictions show that the travel time is accurately represented by
300 the recorded tracer mean velocity. In the accelerating flow cases, Test 1 and 3, the travel time is
301 slightly overestimated compared to the measured concentration profiles. This is a result of using the
302 estimates of travel times based on the trace centroid Reynolds numbers. Predictions made for the
303 different acceleration durations in decelerating flows, Tests 2 & 4, Figures 7 and 9, exhibit dispersion
304 similar to the recorded data. This can be seen in both the spread and peak concentration, where

305   predicted concentration profiles are similar to the measured profiles. Under accelerating flow
306   conditions, Tests 1 & 3, Figure 6 and 8, the predicted temporal concentration profiles exhibit greater
307   dispersion effects than the recorded data, as shown by the greater spread, and more noticeably, in
308   the reduced peak concentrations. Peak concentration values appear to be around 60% of the
309   recorded concentrations for all the acceleration durations, except the late injection during the 60 s
310   acceleration duration, Figure 6d and 8d.

311   Overall, these results show that temporal routing, using actual time for unsteady flow conditions, is
312   accurate for longer acceleration durations and for decelerating flow conditions, agreeing with the
313   results of He and Jackson (2000) and Greenblatt and Moss (2004).

Flow weighted routing

315   This section demonstrates the ability of solute routing in the flow weighted time domain to predict
316   downstream concentrations in unsteady flow conditions (Equation 6). As with the temporal routing,
317   the travel time (from tracer mean velocity) and dispersion coefficients (Equation 4) have been
318   obtained from the equivalent mean steady flow conditions. Note the dispersion coefficients have
319   been converted to dimensionless flow weighted time dispersion coefficients (Equation 7). The
320   predicted flow weighted routing concentration profiles for 5 s, 10 s and 60 s acceleration durations
321   are shown by the solid blue line in Figures 6 to 9 for all the tests. Whilst the routing has been
322   performed in flow weighted time, for ease of comparison the results are presented in actual time.
323   R_t^2 values (denoted ϕ) are given in the upper right corner. The quality of the fit to the data of these
324   predictions made in flow weighted time has a mean R_t^2 value of 0.960, significantly closer to the
325   recorded data than the predictions made using temporal routing (R_t^2 = 0.7).

326   Flow weighted routing travel times exhibit the same features as the temporal routing travel times,
327   for the same rason. . In all test cases, both accelerating and decelerating flow conditions, and across
328   all the transient times studied, the flow weighted routing predictions exhibit very good agreement
329   with both spread and peak concentration. This improvement is most noticeable under accelerating
330   flow conditions, Tests 1 & 3, shown clearly in Figures 6a-c and 8a-c. The benefit and accuracy of
331   using flow weighted time to predict dispersion under time-varying flow conditions, whilst using
332   parameters obtained from steady flow experiments, is very clearly demonstrated.

Optimised dispersion coefficients based on flow-weighted time

334   Dimensionless flow weighted time dispersion coefficients were fit to the laboratory data by
335   optimisation of Equation 6. The predicted optimised flow weighted routing concentration profiles for
336   5 s, 10 s and 60 s acceleration durations are shown by the black dashed line in Figures 6 to 9 for all
337   the tests. Again, whilst the routing has been performed in flow weighted time, for ease of
338   comparison the results are presented in actual time. R_t^2 values (denoted O) are given in the upper
339   right corner. The quality of the optimised fit to the data is very good, with an average R_t^2 value of
340   0.995. The worst individual value, from Test 3 for accelerating flow with the shortest 5 s acceleration
341   duration, had an R_t^2 of 0.982, Figure 8a.

342   The optimised predictions are only slightly more accurate than the predictions made using
343   Equation 4 and Equation 7. All flow weighted routing predictions are very good fits, confirming the
344   suitability of the flow-weighted routing approach for predicting concentrations in unsteady flow
345   conditions and the use of equivalent steady-state parameters to estimate unsteady dispersion. For
346   most engineering applications, all these results are good representations.

Discussion

Predictions based on steady flow non-dimensional dispersion coefficients

The optimised dimensionless flow weighted time dispersion coefficients were converted to the standard dimensionless longitudinal dispersion coefficient, D/ud, and are shown in Table 1, column 10, together with the mean R_t^2 values (column 11) from the five repeat tests. Table 1 also shows the equivalent predicted steady-state dispersion coefficient in column 7 and R_t^2 values when applied using temporal routing in column 8 and flow weighted routing in column 9. This section investigates how the optimised D/ud in unsteady conditions compares to D/ud predicted using the previously published relationship for steady flow conditions, Equation 4 (Hart et al., 2016).

The mean Re over the tracer travel time (Table 1, column 6) signified fully turbulent conditions for all the current unsteady tests, and hence the predicted D/ud values show very little variation, with all values around 0.41, Table 1, column 7. It should be noted that Equation 4 was derived from the optimised longitudinal dispersion coefficient between fluorimeters located at 4.89 m and 13.05 m downstream from the injection location, a longer study reach than was possible for these unsteady flow tests.

The percentage differences between the optimised values and those predicted by Equation 4, (Hart et al., 2016) are given in Table 1, column 12. The decelerating flow conditions, Tests 2 & 4, show greater differences from the steady flow values than the accelerating flow conditions, Tests 1 & 3, with a mean difference of 40%. It is encouraging that the differences confirm the trend suggested by the results of He and Jackson (2000) and Greenblatt and Moss (2004), in that the influence of unsteady conditions reduces with increasing acceleration duration. That is, the slower the flow changes, the more reliably longitudinal dispersion can be approximated to the steady-state values.

The decelerating flow results, Tests 2 & 4, show that all the optimised values of D/Ud obtained from the unsteady flow conditions are less, almost half the value of those obtained from the equivalent steady flow tests. Under accelerating flow conditions, Tests 1 and 3, the average percentage difference between the analysed optimised values and those predicted by Hart et al. (2016) (Table 1, column 12) is approximately zero, with values under predicted for 5 s and 10 s acceleration durations and over predicted for 60 s acceleration duration. Possible reasons for these observed discrepancies are explored in the next subsection.

Limitations of the temporal routing approach

Under decelerating conditions all the values of Optimised D/ud are less than those obtained from the equivalent steady flow tests. It is hypothesised that the lower values are a result of a low turbulence dissipation rate. This leads to residual turbulent fluctuations in the flow after steady mean velocity has been achieved. These residual turbulent fluctuations would generate greater cross-sectional mixing, compared to the level expected for the same steady turbulent flow conditions. This would reduce the effect of differential longitudinal advection, reducing the magnitude of the longitudinal dispersion coefficient.

Under accelerating flow conditions the average percentage difference between the analysed optimised values and those predicted by Hart et al. (2016) is small. The higher percentage differences are probably due to a greater influence of dispersion at the low initial Reynolds number. Results from the steady flow test cases confirm increased values of D/ud as Re reduces. This is further supported by the trend in the percentage differences, from larger positive to larger negative differences as acceleration duration increases.

390   *Multiple peaks*

391   During the initial investigation, temporal concentration profiles with multiple peaks were recorded
392   at the fluorimeter 2.68 m downstream from the injection, as shown in Figure 5a and at all
393   subsequent fluorimeters. These were consistently observed in every trace during the acceleration
394   from initial laminar flow conditions, Test 3. To check whether this was an artefact of the
395   experimental set-up, such as a limitation of the injection system, data from the fluorimeter 0.5 m
396   downstream from the injection was used. Despite the fluorimeter being unable to record the peak
397   concentration, the data shown in Figure 5a confirms the shape of the concentration profile
398   immediately after injection. This clearly shows a single peak, almost symmetrical, with the peak
399   concentration greater than the maximum recordable concentration. Similar concentration profiles
400   were recorded for all the Injection 2 traces conducted in Test 3.

401   Two examples of the concentration profiles with multiple peaks caused by disaggregation of the
402   tracer cloud in Test 3, recorded 2.68 m downstream from the injection, are shown in Figure 10 (grey
403   dots). Figure 10a shows the trace for the shortest acceleration duration, whilst Figure 10b shows the
404   trace for Injection 3 under the 60 s acceleration duration. For this example, travel times from the
405   upstream fluorimeter 0.50 m downstream from the injection, a single peak, to each of the multiple
406   peaks recorded 2.68 m are approximately 7, 10 and 16 s. These are over a distance of 2.18 m, under
407   significantly accelerating flow, as shown by the 10 % increments of flow weighted time. If cross-
408   sectionally well-mixed, this suggests that approximately 5 % of the tracer arrives with a mean
409   velocity of 0.31 m/s, with the majority of tracer, 85 %, travelling at 0.22 m/s and a third discrete
410   pulse, approximately 10 % at 0.14 m/s. The 100 % difference in flow velocity between individual
411   pulses, is similar in magnitude to the spatial differences in velocity recorded by Kurokawa and
412   Morikawa (1986).

413   Assuming that the tracer is cross-sectionally well-mixed in the pipe during the initial laminar flow as
414   the flow is accelerated, the tracer in the centre of the pipe is accelerated more rapidly than the
415   tracer near the pipe boundary. If the flow remains laminar there would be little radial exchange. This
416   acceleration leads to an exaggerated version of the process that creates highly skewed
417   concentration profiles in steady laminar flow, to the point where the dye cloud actually
418   disaggregates. This hypothesis is supported by Kurokawa and Morikawa (1986), whose velocity
419   profiles in Figure 1 show a significant difference between centreline and boundary region velocities
420   prior to the creation of fully turbulent conditions. It is suggested that the multiple peaked tracer
421   profiles are a result of this observed effect. Within the scope of this study, velocity measurements to
422   support this hypothesis were not available and further work is required to fully elucidate the
423   processes.

424   To illustrate the limitations of routing predictions when this disaggregation occurs, the same routing
425   analysis was performed for the data in Figure 10 using a Gaussian distribution fitted to the data
426   recorded at the fluorimeter at 0.5 m for the upstream temporal concentration profile to avoid the
427   problem with off-scale data. The results for data analysis optimised in flow weighted time (black
428   dashed), predictions routed in actual time (red chain dashed), and in flow weighted time (solid blue)
429   are shown. Hart et al. (2016) showed the limitations of employing a Gaussian routing approach for
430   laminar flows and these predictions illustrate similar, although different, concerns. The actual time
431   routed predictions (red chain dashed line) significantly over estimate the longitudinal dispersion,
432   with very low R_t^2 values. The flow weighted time routing predictions are better, but since the
433   upstream concentration profile has a single peak, the ADE-based routing cannot reproduce the
434   recorded multiple peaks, as it does not represent the disaggregation process. This highlights the
435   need for further investigations to explain the cause of the disaggregation during laminar to turbulent

436 flow accelerations. It also illustrates the need to understand the physical processes occurring during
437 low Re flow accelerations in order to make realistic predictions of mixing under these conditions in
438 pipe networks.

Conclusions

440 Experimental studies of longitudinal dispersion in unsteady flows in pipes have been conducted and
441 analysed with the resulting dispersion coefficients compared to those obtained in previous work on
442 steady flows. The analysis has shown the limitations of employing a steady-state routing approach
443 and confirmed that the ability of this method to describe observations decreases with increasing
444 rates of change of discharge. However, employing a routing approach based on the flow weighted
445 time significantly improved predictions for the acceleration durations studied, even when
446 coefficients derived from steady flow experiments are employed in the routing. In practice this
447 means that it is feasible to apply coefficients derived from steady flow experiments within modelling
448 tools, provided that flow-weighted time is adopted in the routing process.

449 From the experiments undertaken in both turbulent to turbulent and laminar to turbulent flows, the
450 results show that smaller values of the longitudinal dispersion coefficient, when compared to the
451 equivalent steady flow conditions, were obtained during decelerating flow. It is suggested that this is
452 a result of residual turbulence in the flow.

453 During acceleration from laminar to turbulent flows a novel disaggregation of the tracer cloud was
454 observed. This occurred during the initial acceleration, and the resulting multiple peaked profiles
455 were recorded at all the locations along the pipe. It is recommended that further detailed studies,
456 including measurements of temporal variations in the velocity and tracer cloud distributions across
457 the pipe, should be undertaken to elucidate and quantify the specific processes that lead to this
458 previously unreported phenomenon.

Data Availability Statement

460 The data, models, and code generated or used during the study are available in a repository online in
461 accordance with funder data retention policies, see Hart et al (2021),
462 https://doi.org/10.15131/shef.data.14135591

Acknowledgements

Notation

468 The following symbols are used in this paper:
469   A =   cross-sectional area;
470   c =   concentration;
471       $c(x,t)$ =   concentration at location x at time t;
472   D =   longitudinal mixing coefficient;
473   D_m =   molecular diffusion coefficient;
474   J =   flow weighted time longitudinal dispersion coefficient;
475   M =   mass of contaminant;
476   Q =   flow rate;
477   Re   =   Reynolds number;
478   R_t^2 =   correlation coefficient;

479	r	=	pipe radius;
480	$S(x, \gamma)$	=	concentration at location x at flow weighted time γ;
481	s	=	distance between measurement points;
482	t	=	time;
483	$\bar{t}$	=	travel time;
484	u	=	velocity;
485	V	=	system volume;
486	x	=	longitudinal distance;
487	Γ	=	distance from the pipe wall;
488	γ	=	integration variable;
489	ϕ	=	non-dimensional flow weighted time;

490 Subscripts

491   i = initial;

492   f = final

References

494 Basha, H.A. and Malaeb, L.N. (2007) Eulerian–Lagrangian Method for Constituent Transport in Water
495   Distribution Networks. *Journal of Hydraulic Engineering*, ASCE, 133(10), 1155-1166.

496 Buchberger, S.G.; Carter, J.T.; Lee, Y., and Schade, T.G. (2003). Random demands, travel times and
497   water quality in deadends. American Water Works Association Research Foundation, Report
498   90963F:470, 2003.

499 Chatwin, P.C. (1970) Approach to normality of concentration distribution of a solute in a solvent
500   flowing along a straight pipe. *Journal of Fluid Mechanics*, 43, 321–352.
501   https://doi.org/10.1017/S0022112070002409

502 Danckwerts, P. V. (1953). Continuous flow systems distribution of residence times. *Chemical*
503   *Engineering Science*, 2(1), 1–13. https://doi.org/10.1016/0009-2509(53)80001-1

504 Fernandez-Sempere, J., Font-Montesinos, R., & Espejo-Alcaraz, O. (1995). Residence time
505   distribution for unsteady-state systems. *Chemical Engineering Science*, 50(2), 223–230.
506   https://doi.org/10.1016/0009-2509(94)00230-O

507 Fischer, H.B., List, J.E., Koh, C. R., Imberger, J., & Brooks, N. H. (1979). *Mixing in Inland and Coastal*
508   *Waters*. Elsevier.

509 Greenblatt, D. & Moss, E.A. (2004). Rapid temporal acceleration of a turbulent pipe flow. *Journal of*
510   *Fluid Mechanics*, 514, 65–75. https://doi.org/10.1017/S0022112004000114

511 Hart, J., Guymer, I., Jones, A.E. & Stovin, V.R. (2013). Longitudinal Dispersion Coefficients within
512   Turbulent and Transitional Pipe Flow. In P. Rowinski (ed.), Experimental and Computational
513   Solutions of Hydraulic Problems, GeoPlanet: Earth and Planetary Sciences,
514   https://doi.org/10.1007/978-3-642-30209-1_28, Springer-Verlag Berlin Heidelberg 2013.

515 Hart, J., Guymer, I., Sonnenwald, F., & Stovin, V. (2016). Residence time distributions for turbulent,
516   critical, and laminar pipe flow. *Journal of Hydraulic Engineering*, 142(9), 04016024.
517   https://doi.org/10.1061/(ASCE)HY.1943-7900.0001146

518 Hart, J., Sonnenwald, F., Guymer, I. (2021). "Temporal Concentration Profiles in Steady and Unsteady
519   Pipe Flow. V1." The University of Sheffield Online Research Data.
520   https://doi.org/10.15131/shef.data.14135591

521 He, S. and Jackson, J.D. (2000). A study of turbulence under conditions of transient flow in a pipe.
522   *Journal of Fluid Mechanics*, 408:1-38. https://doi.org/10.1017/S0022112099007016

523 Holland, J. F., Martin, J. F., Granata, T., Bouchard, V., Quigley, M., & Brown, L. (2004). Effects of
524   wetland depth and flow rate on residence time distribution characteristics. *Ecological*
525   *Engineering*, 23(3), 189–203. https://doi.org/10.1016/j.ecoleng.2004.09.003

526 Kurokawa, J. and Morikawa, M. (1986) Accelerated and decelerated flows in a circular pipe. The
527   Japan Society of Mechanical Engineers, 29(249), 758-765.
528   https://doi.org/10.1299/jsme1958.29.758
529 Leclerc, J., Claudel, S., Lintz, H., Potier, O., & Antoine, B. (2000). Theoretical interpretation of
530   residence-time distribution measurements in industrial processes. *Oil & Gas Science and*
531   *Technology*, 55(2), 159–169. https://doi.org/10.2516/ogst:2000009
532 Levenspiel, O. (1972). *Chemical Reaction Engineering*. John Wiley & Son, Inc.
533 Nauman, E. (1969). Residence time distribution theory for unsteady stirred tank reactors. *Chemical*
534   *Engineering Science*, 24(9), 1461–1470. https://doi.org/10.1016/0009-2509(69)85074-8
535 Romero-Gomez, P. and Choi, C.Y. (2011). Axial Dispersion Coefficients in Laminar Flows of Water-
536   Distribution Systems. *Journal of Hydraulic Engineering*, ASCE, 137(11), 1500-1508.
537   https://doi.org/10.1061/(ASCE)HY.1943-7900.0000432
538 Piazza, S., Blokker E.J.M., Freni, G., Puleo, V. and Sambito, M. (2020). Impact of diffusion and
539   dispersion of contaminants in water distribution networks modelling and monitoring. *Water*
540   *Supply*, 20 (1): 46–58.
541 Taylor, G. I. (1953). Dispersion of soluble matter in solvent flowing slowly through a tube
542   *Proceedings of the Royal Society,* 219(1137), 186–203.
543   https://doi.org/10.1098/rspa.1953.0139
544 Taylor, G. I. (1954) The dispersion of matter in turbulent flow through a pipe. *Proc. R. Soc.*,
545   223(1155), 446–468. https://doi.org/10.1098/rspa.1954.0130
546 Wahl, M. D., Brown, L.C., Soboyejo, A.O., & Dong, B. (2012). Quantifying the hydraulic performance
547   of treatment wetlands using reliability functions. *Ecological Engineering*, 47, 120–125.
548   https://doi.org/10.1016/j.ecoleng.2012.06.009
549 Werner, T.M. & Kadlec, R.H. (1996). Application of residence time distributions to stormwater
550   treatment systems. *Ecological Engineering*, 7(3), 213–234. https://doi.org/10.1016/0925-
551   8574(96)00013-4
552 Young, P., Jakeman, A., & McMurtrie, R. (1980). An instrumental variable method for model order
553   identification. *Automatica*, *16*(3), 281–294. https://doi.org/10.1016/0005-1098(80)90037-0
554
555

556 a) Acceleration duration 2.5 s   b) Acceleration duration 25 s
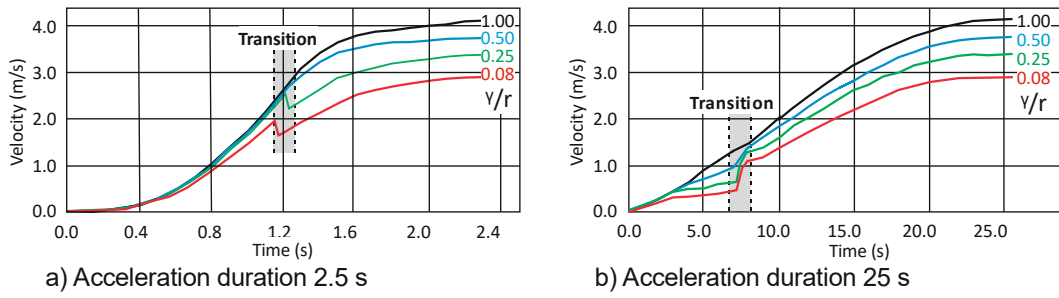
557 Figure 1 – Temporal variations in velocity for accelerated flows in pipes (reproduced from Kurokawa
558 and Morikawa, 1986, Fig. 5, with permission from The Japan Society of Mechanical Engineers) for
559 acceleration duration a) 2.5 s and b) 25 s.

560

561
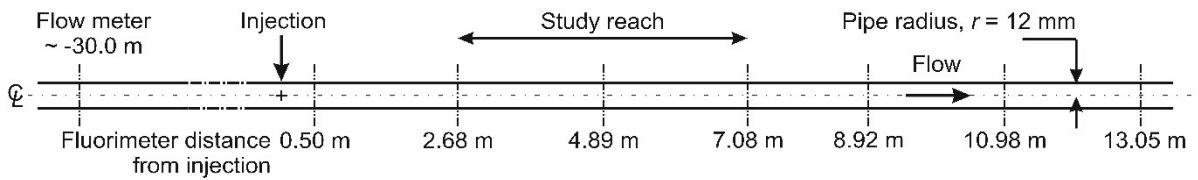
562

563 Figure 2 – Laboratory configuration

564

565
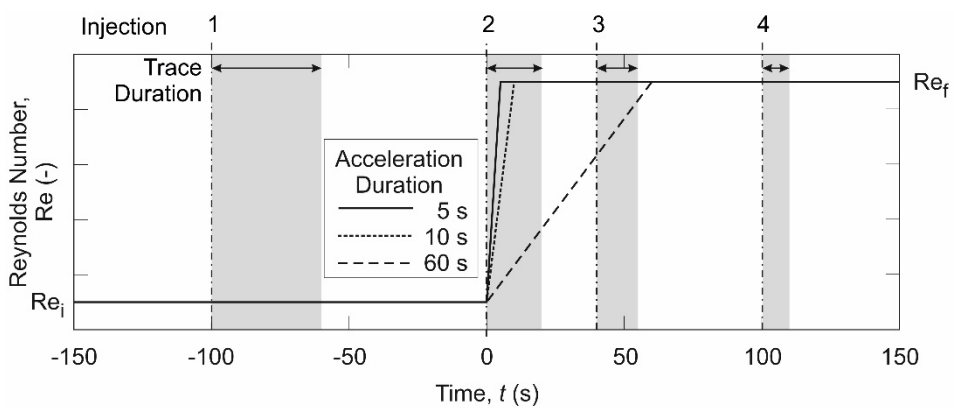
566

567 Figure 3 – Schematic of flow conditions, grey shaded area indicates duration of trace
568 Note: Re_f may be less than Re_i
569
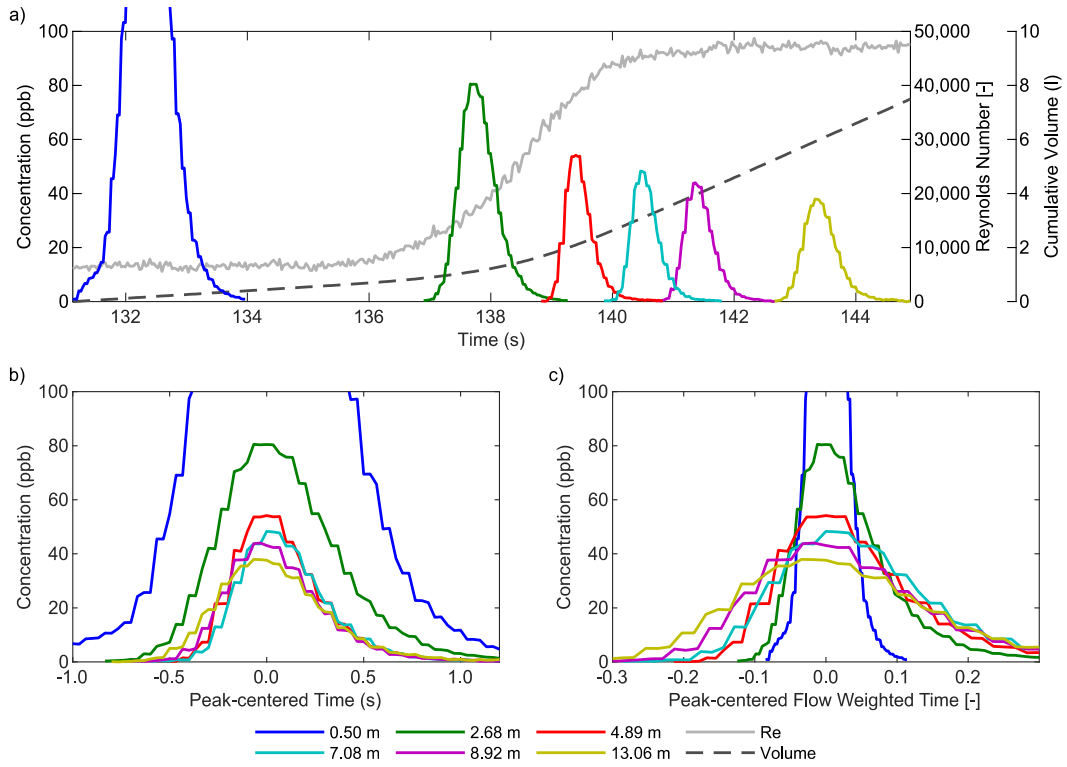
Figure 4 Test 1 with 5 s Acceleration duration: a) temporal variation of measured concentrations, Re and cumulative volume; and peak centred concentrations in b) actual time and c) flow weighted time.
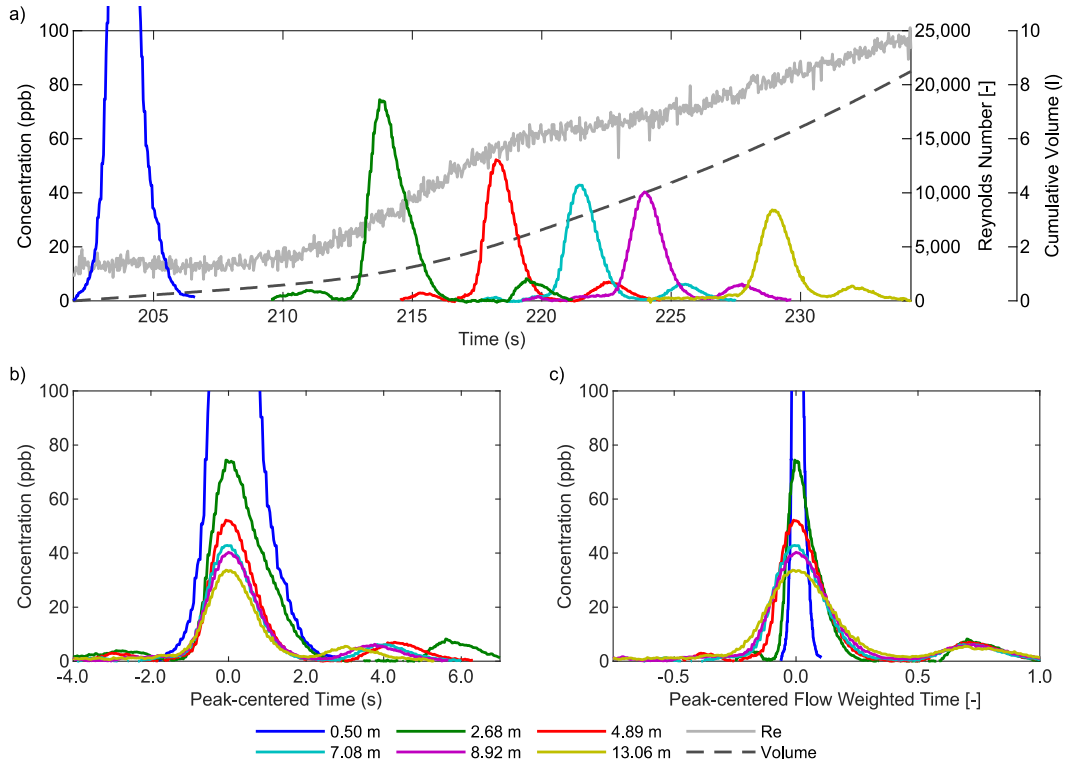
Figure 5 Test 3 with 60 s Acceleration duration: a) temporal variation of measured concentrations, Re and cumulative volume; and peak centred concentrations in b) actual time and c) flow weighted time.

15

578
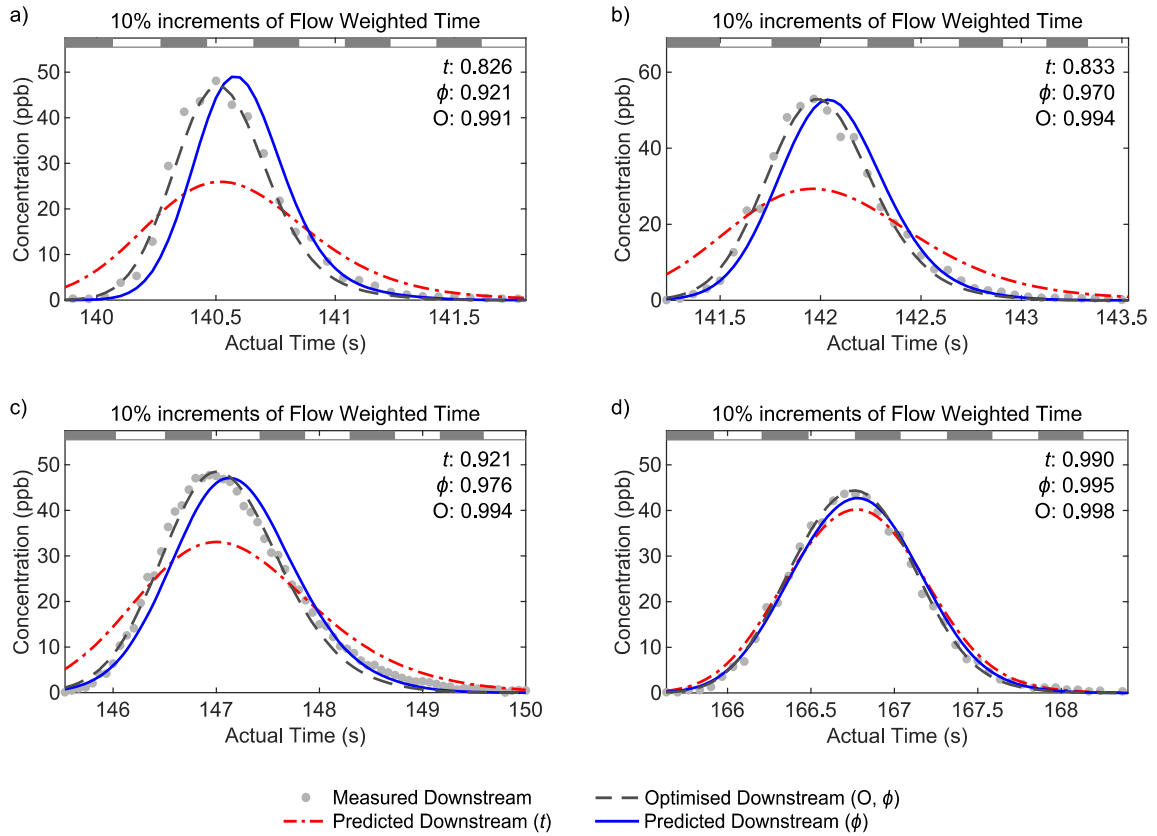
Figure 6 – Test 1: Measured data; Optimised analysis (O) and predicted downstream concentration profiles for a) 5 s, b) 10 s, c) 60 s acceleration duration injection 2, and d) 60 s acceleration duration injection 3. Routing predictions, assuming mean dispersion coefficient, based on Actual Time, (t) and Flow Weighted Time, (ϕ), with R_t^2 shown in the upper right corner.

579

580
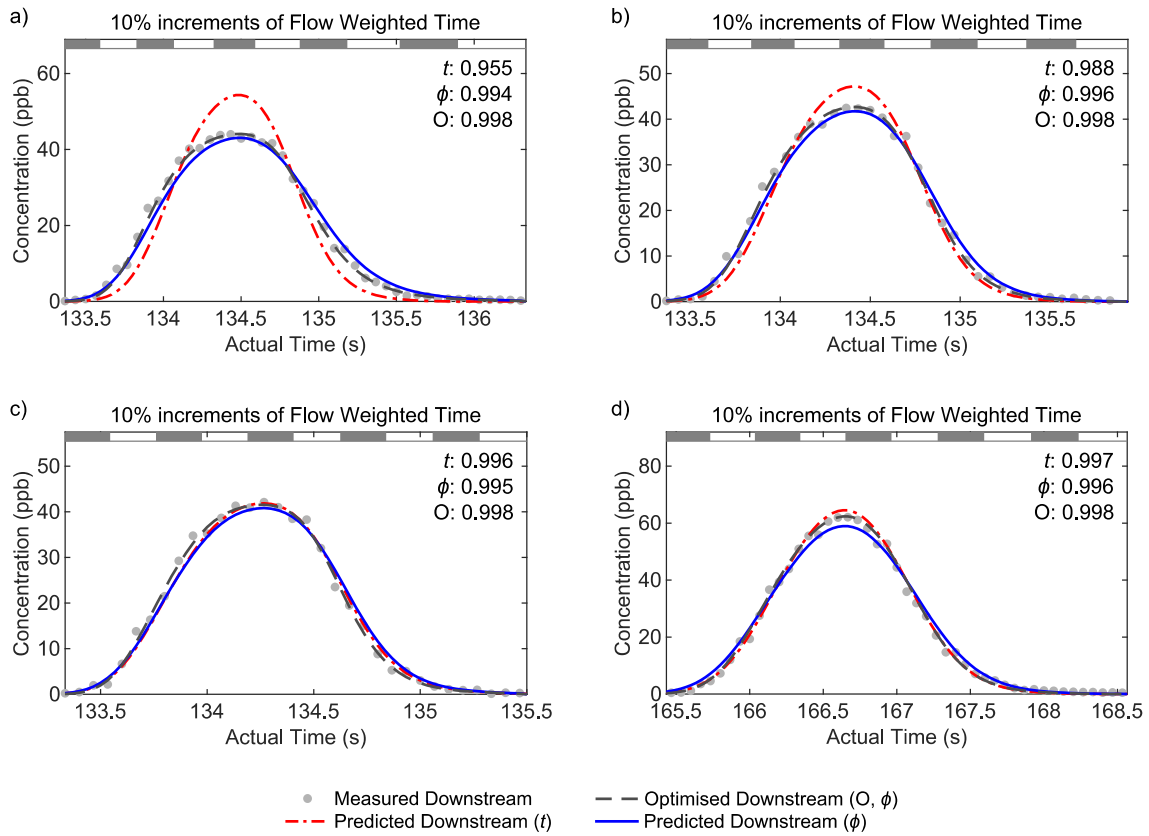
Figure 7 – Test 2: Measured data; Optimised analysis (O) and predicted downstream concentration profiles for a) 5 s, b) 10 s, c) 60 s acceleration duration injection 2, and d) 60 s acceleration duration injection 3. Routing predictions, assuming mean dispersion coefficient, based on Actual Time, (*t*) and Flow Weighted Time, (*ϕ*), with R_t^2 shown in the upper right corner.

581
582

583
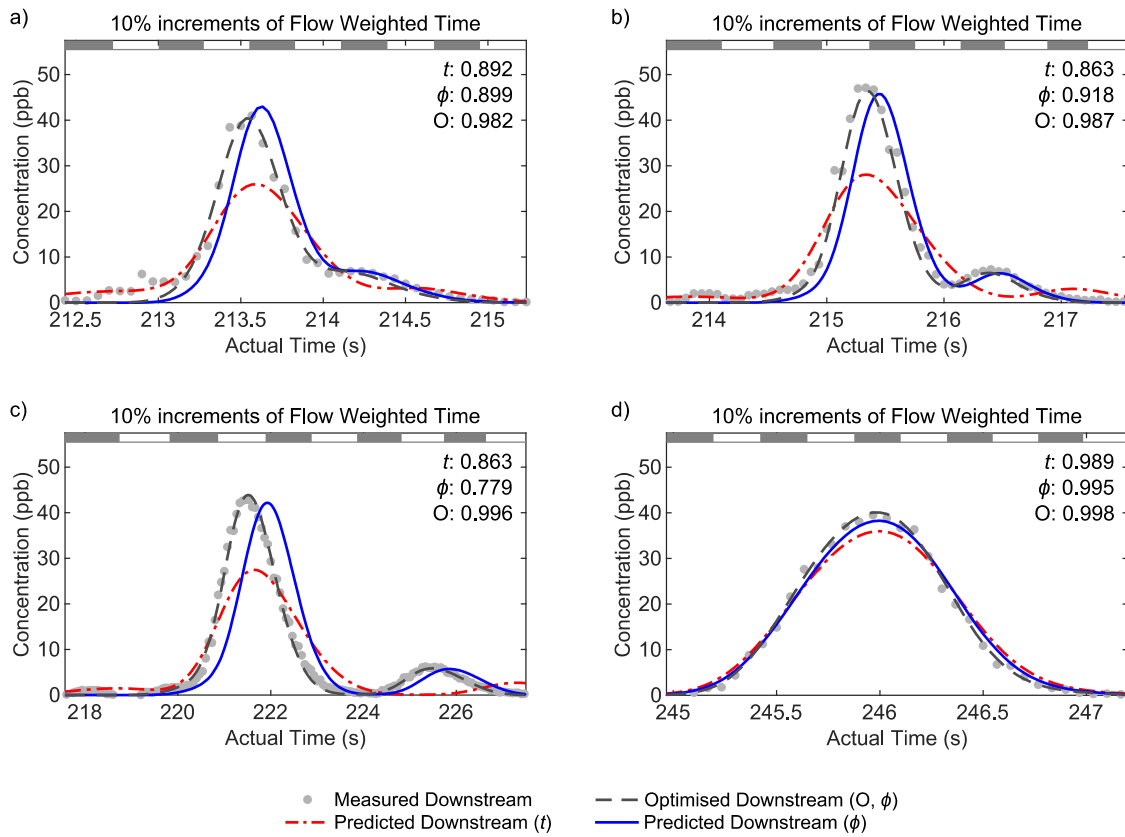
Figure 8 – Test 3: Measured data; Optimised analysis (O) and predicted downstream concentration profiles for a) 5 s, b) 10 s, c) 60 s acceleration duration injection 2, and d) 60 s acceleration duration injection 3. Routing predictions, assuming mean dispersion coefficient, based on Actual Time, (t) and Flow Weighted Time, (ϕ), with R_t^2 shown in the upper right corner.

584
585

586
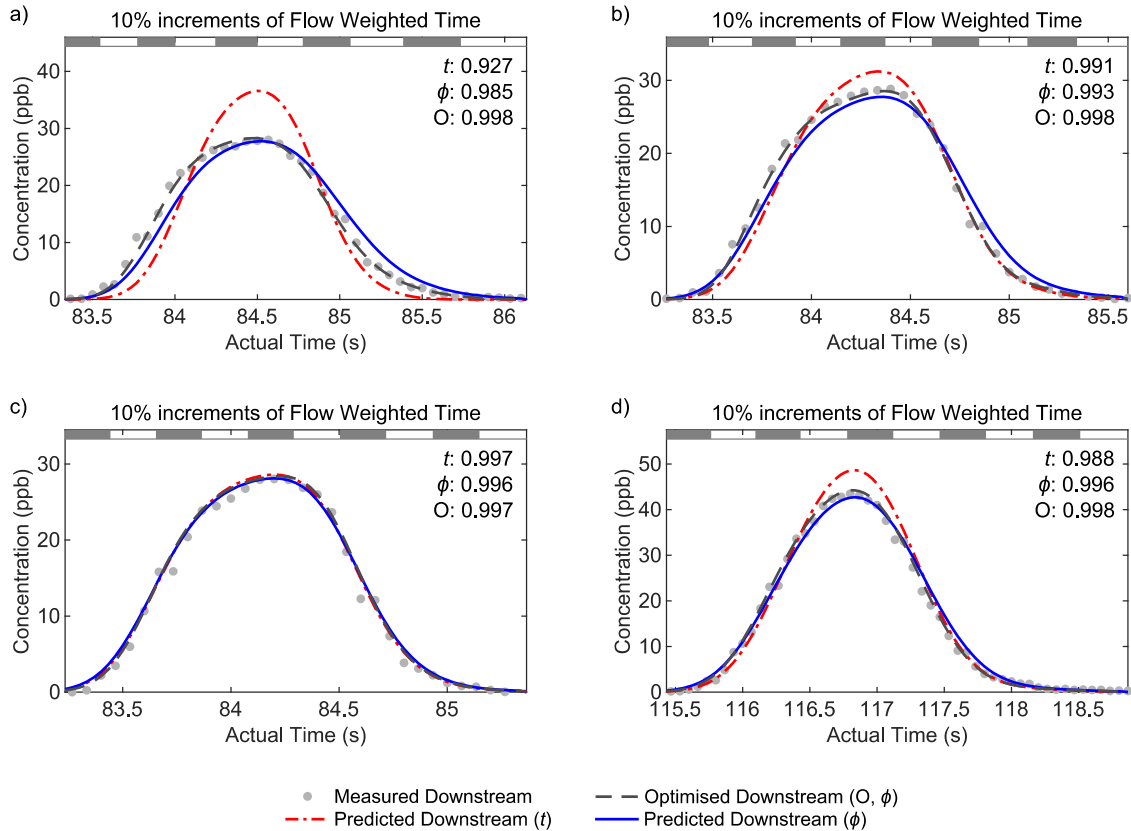
Figure 9 – Test 4: Measured data; Optimised analysis (O) and predicted downstream concentration profiles for a) 5 s, b) 10 s, c) 60 s acceleration duration injection 2, and d) 60 s acceleration duration injection 3. Routing predictions, assuming mean dispersion coefficient, based on Actual Time, (t) and Flow Weighted Time, (ϕ), with R_t^2 shown in the upper right corner.

587

588
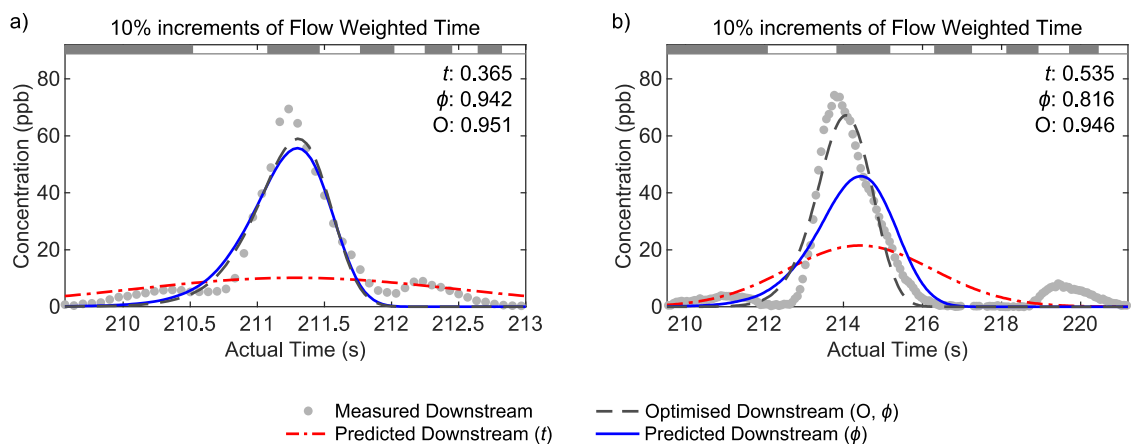
Figure 10 – Test 3 for acceleration from laminar to turbulent flow: Measured data; Optimised analysis (O) and predicted downstream concentration profiles between 0.5 m and 2.68 m for a) 5 s and b) 60 s acceleration duration. Routing predictions, assuming mean dispersion coefficient, based on Actual Time, (t) and Flow Weighted Time, (ϕ), with R_t^2 shown in the upper right corner.

589

590   Table 1 – Details of Experimental Runs

Test	Acceleration duration (s)	Injection	Trace[1] Reynolds Number			Predicted from Equation 4 (Hart et al., 2016)			Optimised Flow Weighted Routing		Diff. (%)
			2.68 m	7.08 m	Mean	D/ud	R_t^2 Temporal Routing (t)	R_t^2 Flow Weighted Routing (ϕ)	D/ud	R_t^2	$\Delta(D/ud)$
1	5	2	18,600	45,700	34,900	0.42	0.211	0.931	0.49	0.991	17
	10	2	14,200	32,600	23,600	0.42	0.284	0.964	0.43	0.994	2
	60	2	8,600	15,200	12,000	0.48	0.710	0.969	0.44	0.994	-8
	60	3	25,900	28,200	27,100	0.42	0.988	0.995	0.32	0.998	-24
2	5	2	46,300	35,800	42,400	0.41	0.943	0.992	0.23	0.998	-44
	10	2	46,500	40,400	43,900	0.41	0.981	0.996	0.23	0.998	-44
	60	2	46,800	45,400	46,200	0.41	0.996	0.996	0.25	0.998	-39
	60	3	27,600	25,500	26,500	0.42	0.992	0.996	0.27	0.998	-36
3	5	2	22,900	49,000	41,300	0.41	0.479	0.817	0.55	0.982	34
	10	2	16,700	35,400	27,800	0.42	0.503	0.930	0.43	0.991	2
	60	2	8,300	16,000	13,300	0.47	0.573	0.806	0.43	0.994	-9
	60	3	30,300	32,200	31,200	0.42	0.991	0.996	0.29	0.998	-31
4	5	2	46,900	36,300	42,800	0.41	0.938	0.987	0.21	0.998	-49
	10	2	47,300	41,300	44,700	0.41	0.982	0.994	0.22	0.998	-46
	60	2	47,300	46,400	46,800	0.41	0.997	0.997	0.29	0.998	-29
	60	3	27,100	24,100	25,500	0.42	0.992	0.996	0.30	0.998	-29
					Mean		0.785	0.960		0.995	
		Standard deviation for repeat traces			≤ 500	< 0.001	≤ 0.057	≤ 0.064	≤ 0.07	≤ 0.004	

591   Test 1 = turbulent to turbulent accelerating flow; Test 2 = turbulent to turbulent decelerating flow

592   Test 3 = laminar to turbulent accelerating flow; Test 4 = turbulent to laminar decelerating flow.

593   [1] Taken from the centroid of temporal concentration profiles at 2.68 m & 7.08 m.